Bulletin of the Seismological Society of America, Vol. 98, No. 4, pp. 2066–2066, August 2008, doi: 10.1785/0120070256

Ⓔ

Short Note

Impact of Earthquake Rupture Extensions on Parameter Estimations of Point-Process Models

by S. Hainzl, A. Christophersen, and B. Enescu

Online Material: Sensitivity to scaling of the d-parameter and to inhomogeneous background activity, and possible correlation between the largest magnitude and estimated α-value.

Abstract Stochastic point processes are widely applied to model spatiotemporal earthquake occurrence. In particular, the epidemic type aftershock sequence (ETAS) model has been shown to successfully reproduce the short-term clustering of earthquakes. An important parameter of the model is the α-value describing the scaling of the aftershock productivity with magnitude of the triggering earthquake according to $10^{\alpha M}$. Fitting of the space-dependent ETAS model to empirical data yields α-values that are typically much smaller than the scaling inverted from more simple stacking of aftershock sequences. We show by means of synthetic simulations that this is likely to result from assuming spatial isotropy of aftershock occurrence that in fact aligns along the mainshock rupture. We fit the space-dependent and space-independent ETAS models to simulations where each earthquake is a line source with an empirical magnitude-length relation. Although the space-time model describes past activity quite well, it overestimates the forecasted earthquake rate. On the other hand, the application of the space-independent ETAS model predicts future seismicity well and can therefore be applied for forecasting purposes. Our test for the observed aftershock sequence following the 1992 M 7.3 Landers earthquake supports these results.

Introduction

In the recent past, strong efforts have been undertaken to test our present-day ability to forecast earthquakes, for example, within the Regional Earthquake Likelihood Models (Hough and Olsen, 2007) and the Collaboratory for the Study of Earthquake Predictability projects (http://scecdata.usc.edu/csep). Within this context, the forecasting of aftershocks is also of interest (e.g., Gerstenberger *et al.*, 2005 and the Seismic Early Warning for Europe [SAFER] project, http://www.saferproject.net/index.htm). Forecasting of aftershocks seems to be feasible because of two well-known empirical laws: (1) the aftershock rate generally decays according to the Omori–Utsu law, $\sim(c+t)^{-p}$, where c and p are constants and t is the elapsed time since the main event (for a review, see Utsu *et al.*, 1995); (2) the aftershock area grows exponentially with mainshock magnitude M (Utsu and Seki, 1955) and so does the number of aftershocks (Kanamori and Anderson, 1975), leading to the productivity proportional to $10^{\alpha M}$.

The epidemic type aftershock sequence (ETAS) model is a stochastic point-process model that builds on the aforementioned empirical characteristics and takes stationary seismicity and secondary aftershocks into account (Ogata, 1988; Helmstetter and Sornette, 2002). In the ETAS model, each earthquake has some magnitude-dependent ability to trigger aftershocks according to $K10^{\alpha(M-M_{\min})}$, where K is a constant and $M_{\min}$ is the lower magnitude cutoff of the earthquakes under consideration. In this context and throughout the whole article, aftershocks are defined as triggered events independent of whether they are smaller or larger than their parent earthquakes. The total occurrence rate of earthquakes is given by

$$\lambda(t,x,y)=\mu+\sum_{i:t_i<t}\frac{K10^{\alpha(M_i-M_{\min})}}{(t-t_i+c)^p}f_i(x-x_i,y-y_i), \quad (1)$$

where μ is the background rate and $f_i(x,y)$ is a normalized function, which describes the spatial probability distribution

of triggered aftershocks. Frequently, the isotropic power-law kernel,

$$f(x,y) = \frac{(q-1)d^{2(q-1)}}{\pi[x^2+y^2+d^2]^q}, \tag{2}$$

is used with the two parameters q and d (Console *et al.*, 2003, 2006; Zhuang *et al.*, 2004; Helmstetter *et al.*, 2005). A q-value of 1.5 would be consistent with static stress triggering, which decays according to $\sim r^{-3}$. To account for anisotropy, a more general form was originally proposed by Ogata (1998), where x^2+y^2 is replaced by $(x,y)\mathbf{S}(x,y)^t$. Here, $\mathbf{S}$ is a 2×2 positive definite symmetric matrix, and $(x,y)^t$ indicates the vector transpose relative to the centroid of the aftershock cloud. The quadratic form allows aftershocks to be spatially distributed with ellipsoidal contours. However, as the inversion of $\mathbf{S}$ from earthquake data is not straightforward because in general $\mathbf{S}$ and the centroid position must be estimated for each event independently, an identity matrix is usually assumed leading to equation (2).

A number of studies have addressed how the number of aftershocks produced by a mainshock depends on its magnitude (Kanamori and Anderson, 1975; Yamanaka and Shimazaki, 1990; Felzer *et al.*, 2002, 2004). While there is good evidence that the productivity grows exponentially with M as $\sim 10^{\alpha M}$, the exact value of α varies substantially between empirical studies, in particular, between windows-based cluster definitions and ETAS-model fits. Although Christophersen and Smith (2008) showed that the inferred α-value depends on the applied magnitude scaling of the spatial windows, the former class typically yields values close to 1: Helmstetter (2003) obtained that $0.7 < \alpha < 0.9$ for southern California, while Helmstetter *et al.* (2005) found $\alpha = 1.05 \pm 0.05$ for the same region. An α-value close to 1 would imply that the number of aftershocks scales in a similar way as the mainshock rupture area. This is also in general agreement with the scattered α-values around 1, which are obtained by the space-independent ETAS model ($f(x,y) = 1$) for various sequences in Japan (Ogata, 1992). On the other hand, using space-dependent ETAS models and inverting for the model parameters yields significantly lower values; for example, Zhuang *et al.* (2004) found that $\alpha \simeq 0.6$ for Japan (1926–1999 $M \geq 4.2$ earthquakes), Zhuang *et al.* (2005) found $\alpha = 0.7 \pm 0.05$ for Taiwan (1941–2001 $M \geq 5.3$ earthquakes), while Console *et al.* (2003) obtained $\alpha = 0.42$ for Italy (1987–2000 $M \geq 2$ earthquakes).

In this study, we show that the apparently smaller values inverted by means of the space-time ETAS models are likely to result from neglecting the earthquake rupture extensions because earthquakes are treated as point sources with a spatially isotropic probability function for aftershock triggering. If the spatial extent of earthquake sources is not taken into account, forecasting of ongoing aftershock activity is erroneous. To show this, we will analyze ETAS simulations with realistic spatial aftershock distribution in the section entitled Synthetic Simulations and study the Landers aftershock sequence in the section entitled Landers Aftershock Sequence.

Synthetic Simulations

We used Monte Carlo simulations of the ETAS model as described by equations (1) and (2). To choose appropriate input parameters for these simulations, we fitted the ETAS model to the seismicity preceding the 1992 M 7.3 Landers, California, earthquake. We used the relocated data set by Hauksson *et al.* (2003) for the region −119° W–−115.5° W and 32.5° N–36.5° N and the time interval between $t_1 =$ 1 January 1984 and $t_2 =$ 27 June 1992 (downloaded from the Southern California Earthquake Data Center [SCEDC] web site at http://www.data.scec.org/research/altcatalogs.html). The catalog included $N = 1537$ earthquakes with $M \geq 3$. We optimized the parameters μ, K, c, p, q, and d by a maximum likelihood method that is performed according to Ogata (1992), using the Davidon–Fletcher–Powell method (e.g., Fletcher and Powell [1963]). The α-parameter was thereby set to the middle of previous estimations, $\alpha = 0.8$. As discussed later, a free α would have been underestimated by the space-dependent ETAS model.

The likelihood function can be written as

$$\begin{aligned}\ln L &= \sum_{i=1}^{N} \ln \lambda(t_i,x_i,y_i) - \int_{t_1}^{t_2}\int_{x_1}^{x_2}\int_{y_1}^{y_2} \lambda(t,x,y)\,d\,x\,d\,y\,d\,t \\ &= \sum_{i=1}^{N} \ln \lambda(t_i,x_i,y_i) - \mu(x_2-x_1)(y_2-y_1) \\ &\quad - \int_{t_1}^{t_2} \sum_{i:t_i<t} \frac{K10^{\alpha(M_i-M_{\min})}}{(t-t_i+c)^p}\,d\,t \end{aligned} \tag{3}$$

(Ogata, 1998; Daley and Vere-Jones, 2003). The inverted values are summarized in Table 1. Note that for the simulations, we set the background rate to 0 instead of the inverted small value of 0.039 (day^{-1}).

We produced Monte Carlo simulations of the ETAS model using the inverse (transform) method (see, e.g., Daley and Vere-Jones, 2003). A mainshock of M 7.3 was assumed to occur at time 0. Aftershock magnitudes were drawn from a

Table 1
Summary of the Model Input Parameters for the ETAS Simulations

$M_{\text{main}}(t=0)$	$M_{\min}$	μ (day^{-1})	K	c (days)	α	p	q	d (km)
7.3	3.0	0	0.0157	0.0016	0.8	0.99	1.45	0.53

Gutenberg–Richter frequency-magnitude distribution with $b = 1$ and a maximum magnitude of 7.0. To account for the spatial extension of each rupture, we assumed that the rupture length L scales with the earthquake magnitude according to the empirical relation of Wells and Coppersmith (1994): $L = \sqrt{A} = \sqrt{10^{-3.49+0.91M}}$ km (where A is the rupture area) and took the form of a line with random orientation in space. Each point on the rupture could equally trigger aftershocks according to the isotropic kernel. This was done by first selecting a random point on the rupture (line segment) and then selecting a random point relative to this location according to the spatial probability function of equation (2). An example for such a simulated aftershock sequence is shown in Figure 1 in comparison to the Landers aftershock sequence.

We analyzed the Monte Carlo simulations with two different inversion strategies: (A) inversion by means of the space-time ETAS model and (B) inversion by the space-independent model. In the latter case, equation (2) is replaced by $f(x, y) = 1$.

At first, we investigated whether the input parameters could be obtained by maximizing the likelihood function (equation 3). For 100 simulations, Figure 2 shows the results for the inversion of the first 10 days of aftershocks (typically about 1000 events). The results are striking: the procedure (B) that neglected all information about the spatial triggering results in an unbiased estimation of all parameters ($K = 0.015 \pm 0.002$, $c = 0.0017 \pm 0.0004$ days, $\alpha = 0.81 \pm 0.02$, $p = 0.99 \pm 0.02$). By contrast, procedure (A) that used the correct model besides the fact that earthquakes were taken as point sources leads to significantly wrong estimations. In particular, the parameter $K = 0.037 \pm 0.002$ is estimated significantly too high and $\alpha = 0.55 \pm 0.02$ too low. Note that both parameter estimations are not independent but highly correlated. A trade-off between both parameters is expected because the number of events is increasing rapidly for lower magnitude levels (according to the Gutenberg–Richter relation $N \sim 10^{-bM}$). If α becomes lower, then the more frequent smaller events contribute significantly more to the aftershock productivity and K must be smaller to result in the same total (observed) number of events.

We performed a test with simulations where we use point instead of line sources for each earthquake. This test shows that the parameter mismatch is only due to the anisotropy of the aftershock clouds. As already suggested as one possibility by Helmstetter *et al.* (2006), the explanation is that a smaller α-value gives more importance to secondary aftershocks in the isotropic space-time ETAS model, and thus, the model can better adapt to the anisotropic, spatially elongated seismicity distribution triggered by the mainshock.

Ⓔ As presented in the supplemental material in the electronic edition of *BSSA*, we performed additional tests concerning the robustness of these results. Although we cannot perform an exhaustive testing of all of the possibilities that might have an impact on the α-estimation (see discussion by Helmstetter *et al.* (2006)), our analysis indicates that neither the magnitude range, observational errors, nor spatial heterogeneities of the background activity affect the parameter estimation significantly. It is, however, found that using an isotropic spatial kernel (equation 2), where d is scaling with the mainshock magnitude, leads to a slightly better estimation than assuming a constant d-value. This agrees in principle with the observation that estimates with vari-

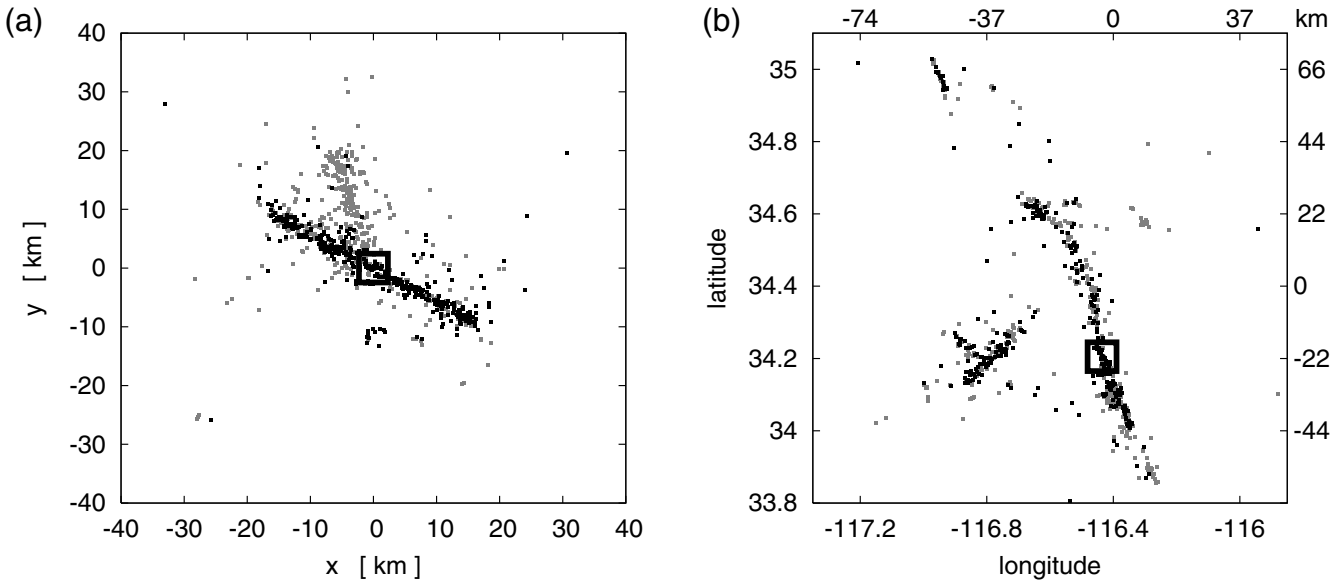

Figure 1. Example of (a) an ETAS simulation and (b) Landers aftershocks. Both plots show all $M \geq 3$ aftershocks occurred within the first 10 days, where the aftershocks of the first 24 hr are plotted in black. In each plot, the epicenter of the mainshock is additionally marked by a big square.

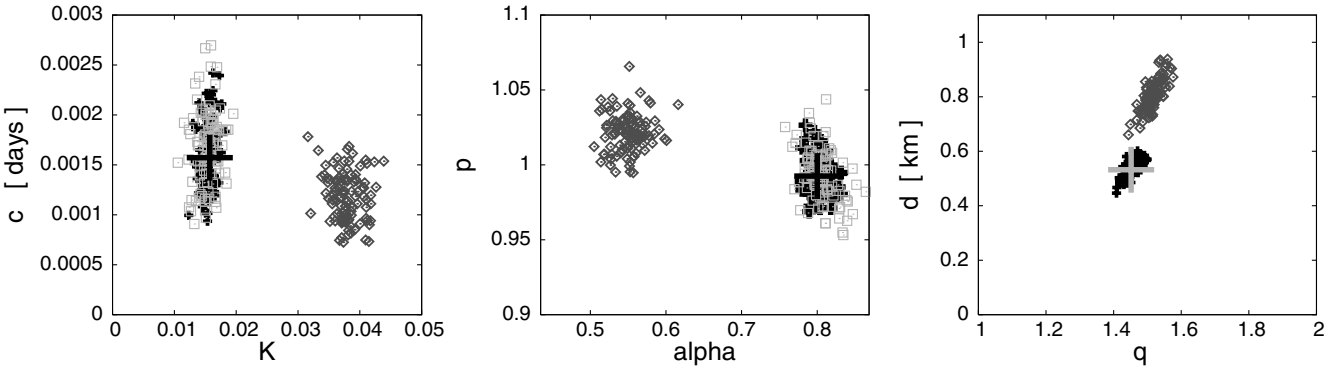

Figure 2. Estimated parameters by fitting the space-dependent (diamonds) and space-independent (squares) ETAS models to the first 10 days of aftershocks for 100 different stochastic simulations. The true values are indicated by the large crosses. For comparison, the test results for simulations with isotropic aftershock distributions are additionally shown for the space-dependent ETAS model (small black crosses, partially overlaid by the squares). In this case, the model yields unbiased estimations.

able $d(M)$ lead to higher α-values (Zhuang *et al.*, 2004) than those with constant d-values (Console *et al.* 2003).

Forecasting Ability

We now show that the forecasting ability is strongly affected if the anisotropy of aftershock clouds is ignored. We estimated the ETAS parameters from the aftershocks of the first $T = 1$ day, 1 week, and 1 month and used the inverted parameters to forecast the expected number of events for the subsequent N days. The forecasts were done again by Monte Carlo simulations: for each inverted parameter set and given precursory activity, we calculated the average number of events that are simulated for the next N days in 10^4 different stochastic realizations. In the simulations, we took into account aftershocks of aftershocks triggered within the prediction period, which are known to significantly contribute to the overall rate in the ETAS model (Helmstetter *et al.*, 2003). The ratio between the forecasted and the real number of earthquakes is shown in Figure 3 together with its standard deviation. It can be clearly seen that while the space-independent approach leads to good forecasts (ratios $\approx$1), the space-dependent measurements largely overestimate the earthquake rates. In particular, the ratio of forecasted and observed events grows exponentially with time for parameter estimation following shortly after the mainshock; even parameter estimations 30 days after the mainshock still yield forecasted rates more than twice the observations.

Besides the temporal predictability, we also tested the spatial forecasting ability. We applied three different procedures:

1. Using the space-time ETAS model for inversion and prediction.
2. Using the space-independent ETAS model for the inversion of K, c, α, and p. The spatial triggering was twofold. Aftershocks were allowed to spatially trigger secondary aftershocks according to equation (2), where the two parameters q and d were taken from the estimates of the space-time ETAS model. The direct aftershocks of the mainshocks were assumed to be triggered on a spatial probability map, which resulted from smoothing of the first 0.1 days of aftershocks (a minimum number of 50 events) by means of
   (a) An isotropic adaptive Gaussian kernel according to Helmstetter *et al.* (2007), where we chose two neighbors for calculating the standard deviation.
   (b) The power-law kernel in equation (2) with inverted parameters q and d.

We calculated the coefficient r of the linear spatial correlation between the estimated $\tilde{p}_i$ and true p_i probability values at the N grid points in a 100×100-km box surrounding the mainshock (with grid spacing of 1 km) after 1, 5, and 10 days. Mathematically, it is defined as

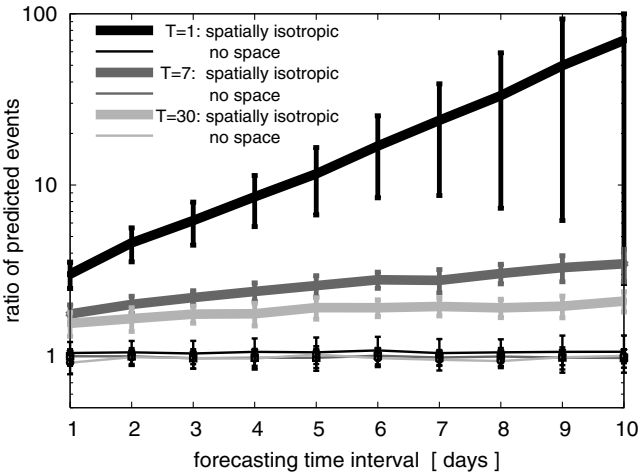

Figure 3. The ratio between the forecasted versus the true number of events as a function of the prediction time. The curves show average values together with their standard deviation for the space-dependent and space-independent ETAS models for different starting times T of the forecasts.

Table 2
Linear Correlation Coefficient between the Predicted and the True Spatial Probability Distribution for the Next 24 hr as a Function of Time after the Mainshock

	1 day after Mainshock			5 days after Mainshock			10 days after Mainshock		
Model	$\bar{r}$	r_{50}	σ_r	$\bar{r}$	r_{50}	σ_r	$\bar{r}$	r_{50}	σ_r
1	0.88	0.89	0.02	0.94	0.94	0.02	0.94	0.94	0.02
2(a)	0.85	0.86	0.05	0.92	0.94	0.07	0.92	0.94	0.06
2(b)	0.89	0.90	0.05	0.93	0.95	0.07	0.93	0.95	0.06

Mean $\bar{r}$, median r_{50}, and standard deviation σ_r.

$r = \sum_i^N (\tilde{p}_i - \langle \tilde{p} \rangle)(p_i - \langle p \rangle)/(N\sigma_{\tilde{p}}\sigma_p)$, where $\langle\rangle$ and σ_p denote the spatial average and standard deviation, respectively. The result, which is not significantly depending on the grid spacing, is shown in Table 2 for 100 different ETAS simulations. All three procedures led to comparable high correlations. Although the procedure 2(b) led to slightly better median values, this procedure as well as 2(a) sometimes had quite bad estimations, which is reflected in the larger standard deviations. These were caused by large aftershocks with nonnegligible rupture extensions. To improve the estimation, secondary large aftershocks must therefore also be treated similarly to the mainshock. However, this would lead to a complex algorithm with additional parameters (a magnitude cutoff to define the lower bound for smoothing, the time interval for smoothing, and a minimum event number for smoothing; see, for example, Helmstetter *et al.* 2007). Thus, the straightforward and robust prediction of the spatial distribution by means of the space-time ETAS model (procedure 1) seems to be superior.

Landers Aftershock Sequence

Finally, we applied the same procedure to the observed Landers aftershock sequence. The Landers mainshock occurred on the 28 June 1992 and its epicenter was located at longitude −116.44 and latitude 34.20 and a magnitude of 7.3. We analyzed the relocated earthquake catalog of Hauksson *et al.* (2003) for the region −117.5° W–−115.5° W and 33.25° N–35.5°N and the time interval between $t_1 =$ 28 June 1991 and $t_2 =$ 28 June 1993 (SCEDC web site, http://www.data.scec.org/research/altcatalogs.html). The ETAS parameters were inverted for $M \geq 3$ events after each 24 hr subsequent to the mainshock, that is, at times $T_i = t_M + i$ days. However, the maximization of the log-likelihood function (equation 3) was done only for aftershocks occurring after the first 12 hr (i.e., within $[t_M + 0.5, T_i]$) to account for possible incompleteness of the recordings in the first time interval (Kagan, 2004). We chose 12 hr in agreement with the estimation of Helmstetter *et al.* (2005) for the time of incompleteness for $M \geq 3$ in southern California. However, all of the earthquakes that occurred before $t_M + 0.5$ days (also foreshocks) were taken into account to calculate the rates at times larger than that. More precisely, the local rates defined by equation (1) were calculated from all preceding events (since 28 June 1991) whereas the log-likelihood function (equation 3) was calculated only for the N events that occurred in the time period $(t_M + 0.5, T_i)$. Table 3 shows the estimated parameters (mean and standard deviation of the 90 estimations with $T_i = 1, \ldots 90$ days) in comparison to the values of the background model. The background values were estimated from the seismic activity preceding the mainshock in the larger region −119° W–−115.5° W and 32.5° N–36.5° N within the time interval between $t_1 =$ 1 January 1984 and $t_2 =$ 27 June 1992. In contrast to the estimates given in Table 1, we also inverted the α-parameter from the data.

The parameter estimations differ significantly between the space-dependent and space-independent ETAS models.

Table 3
The Estimated ETAS Parameters for the Background and Landers Aftershock Activity

	Space-Independent Model		Space-Dependent Model	
	Aftershocks	Background	Aftershocks	Background
K	0.0067 ± 0.0022	0.021	0.097 ± 0.026	0.040
c (days)	0.013 ± 0.038	0.003	0.029 ± 0.028	0.001
α	0.99 ± 0.05	0.70	0.24 ± 0.03	0.36
p	1.07 ± 0.15	1.05	1.05 ± 0.11	0.98
q	—	—	1.49 ± 0.02	1.44
d (km)	—	—	0.50 ± 0.06	0.48

The parameters for the Landers aftershock activity are estimated with their standard deviations from the time intervals $(0.5, T_n)$ days with $T_n = 1, 2, \ldots 90$ days.

Similar to our synthetic study, the inverted K-value is much higher and the α-value much smaller in the case of the space-time model than for the space-independent model, whereas the c- and p-values are similar. The estimations are stable after approximately 4 days after the mainshock; however, they are not always similar to the premainshock values. In particular, the c-value for the Landers sequence is larger than that estimated from the preceding seismicity. The α-parameter values for the background seismicity and Landers aftershocks are also significantly different. However, both α-values inverted by the space-independent model are now in good agreement with the range of estimations resulting from direct fits (Helmstetter, 2003; Helmstetter *et al.*, 2005). Furthermore, it is interesting to note that the q-value is close to 1.5 for both data sets. This corresponds to a decay with distance according to $\sim r^{-3}$. Thus, our result indicates that aftershocks around the fault zone seem to be triggered by static rather than, as recently claimed, by dynamic stress changes (Felzer and Brodsky, 2006).

Finally, we tested the forecasting ability for both models. In the same way as described for the synthetic simulations (see the section entitled Landers Aftershock Sequence), we forecasted the number of $M \geq 3$ earthquakes in the next 24 hr based on the aftershocks that had already occurred. For the simulation-based forecasts, we used a maximum aftershock magnitude of 6.3 to stabilize the forecasts by avoiding that one simulation, which consists of a very large aftershock triggering a huge number of secondary events, can dominate the ensemble forecast. Similar results are obtained for the median value in the case of an unrestricted maximum magnitude. The b-value for the simulations was estimated at each time step T_i from the preceding aftershock activity by the maximum likelihood method (Aki, 1965) yielding values between 0.89 and 0.94. In addition to the previous models, we also calculated the forecasts based on the background models, that is, for the case that the parameters were not updated during the ongoing aftershock sequence. The resulting forecasts are shown in Figure 4 where they are compared with the observations. It is obvious that the space-independent ETAS model best predicts—at least in the first days—the occurred rates; in particular, the forecast based on updated parameters performs the best. On the other hand, the space-time ETAS model leads to significantly biased estimations. The background model clearly underpredicts and the updated version overpredicts the real aftershock numbers. Please note that a more detailed comparative test of the spatiotemporal forecasts for the Landers aftershock sequence will be done in a forthcoming article.

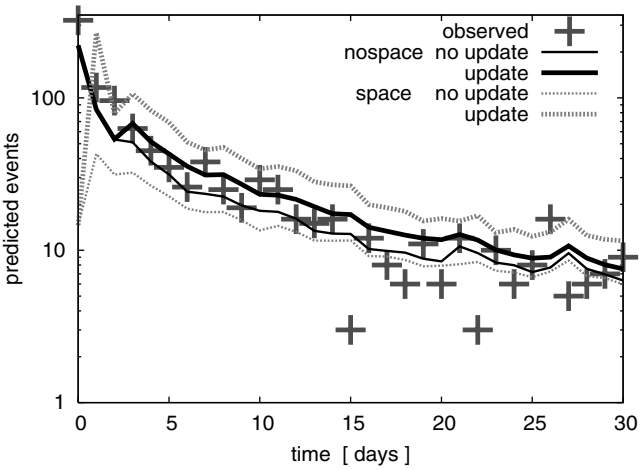

Figure 4. The forecasted number of $M \geq 3$ aftershocks within the next 24 hr as a function of time after the Landers mainshock. The crosses indicate the observed number of events and the different curves refer to the different forecasting procedures.

Summary and Conclusions

The ETAS model is a very powerful model in describing short-time clustering of earthquakes. Here we show, however, that the estimations of the space-time ETAS model can be strongly biased if earthquakes are treated as point sources with spatially isotropic aftershock probability. In principle, anisotropic aftershock distributions can be considered in the space-time ETAS model, for example, by an ellipsoidal instead of a radial distribution (Ogata, 1988; Schoenberg, 2003; Ogata and Zhuang, 2006). However, this requires additional assumptions and a nontrivial fit to the aftershock distribution. Therefore, the anisotropy is often neglected, which explains why the scaling parameter α for the aftershock productivity is generally found to be significantly smaller if it is estimated by a space-dependent point-process model rather than by stacking procedures. Using synthetic aftershock sequences and the test case of the Landers sequence, we have demonstrated that neglecting this problem can lead to a drastic drop of the forecasting ability of the ETAS model. As a result of our study, we propose an optimized strategy for using the ETAS model for earthquake forecasting: (1) forecast of the number of events by means of applying the space-independent ETAS model to a region surrounding the mainshock (in order to invert for K, c, α, and p) and (2) estimate the spatial probability distribution based on the estimation of the space-time model. In the future, we will compare this procedure to alternative model forecasts and test the forecasts for a number of different aftershock sequences.

Acknowledgments

This work is part of the European projects SAFER (Seismic Early Warning for Europe, Contract Number 036935) and NERIES (Network of Research Infrastructures for European Seismology, Contract Number 026130). We are grateful to the associate editor, Stefan Wiemer, and an anonymous referee for the detailed report and helpful recommendations. Finally, we are thankful to Jochen Woessner for stimulating this research by his forecasting tests.

References

Aki, K. (1965). Maximum likelihood estimate of b in the formula $\log N = a - bM$ and its confidence limits, *Bull. Earthq. Res. Inst.* **43,** 237–239.

Christophersen, A., and E. G. C. Smith (2008). Foreshock rates from aftershock abundance with different search algorithms, *Bull. Seismol. Soc. Am.* (in press).

Console, R., M. Murru, and A. M. Lombardi (2003). Refining earthquake clustering models, *J. Geophys. Res.* **108,** no. B10, 2468, doi 10.1029/2002JB002130.

Console, R., M. Murru, F. Catalli, and G. Falcone (2006). Real time forecasts through an earthquake clustering model constrained by the rate-and-state constitutive law: comparison with a purely stochastic ETAS model, *Seism. Res. Lett.* **78,** 49–56.

Daley, D. J., and D. Vere-Jones (2003). *Elementary Theory and Methods*, in An Introduction to the Theory of Point Processes, Second Ed., Vol. **1**, Springer, New York.

Felzer, K. R., and E. E. Brodsky (2006). Decay of aftershock density with distance indicates triggering by dynamic stress, *Nature* **441,** no. 7094, 735–738.

Felzer, K. R., R. E. Abercrombie, and G. Ekstrom (2004). A common origin for aftershocks, foreshocks, and multiplets, *Bull. Seismol. Soc. Am.* **94,** no. 1, 88–98.

Felzer, K. R., T. W. Becker, R. E. Abercrombie, G. Ekstrom, and J. R. Rice (2002). Triggering of the 1999 M-W 7.1 Hector Mine earthquake by aftershocks of the 1992 M-W 7.3 Landers earthquake, *J. Geophys. Res.* **107,** no. B9, 2190.

Fletcher, R., and M. J. D. Powell (1963). A rapidly convergent descent method for minimization, *Comput. J.* **6,** 163–168.

Gerstenberger, M. C., S. Wiemer, L. M. Jones, and P. A. Reasenberg (2005). Real-time forecasts of tomorrow's earthquakes in California, *Nature* **435,** 328–331.

Hauksson, E., W-C. Chi, and P. Shearer (2003). Comprehensive waveform cross-correlation of southern California seismograms: part 1. Refined hypocenters obtained using the double-difference method and tectonic implications (abstract), in *Proc. Fall Ann. Meeting, American Geophysical Union*, 8–12 December 2003, San Francisco, CA.

Helmstetter, A. (2003). Is earthquake triggering driven by small earthquakes?, *Phys. Rev. Lett.* **91,** no. 5, 058501.

Helmstetter, A., and D. Sornette (2002). Subcritical and supercritical regimes in epidemic models of earthquake aftershocks, *J. Geophys. Res.* **107,** no. B10, 2237.

Helmstetter, A., Y. Y. Kagan, and D. D. Jackson (2005). Importance of small earthquakes for stress transfers and earthquake triggering, *J. Geophys. Res.* **110,** B05S08, doi 10.29/2004JB003286.

Helmstetter, A., Y. Y. Kagan, and D. D. Jackson (2006). Comparison of short-term and time-independent earthquake forecast models for southern California, *Bull. Seismol. Soc. Am.* **96,** no. 1, 90–106.

Helmstetter, A., Y. Y. Kagan, and D. D. Jackson (2007). High-resolution time-independent grid-based forecast for $M \geq 5$ earthquakes in California, *Seism. Res. Lett.* **78,** 78–86.

Helmstetter, A., D. Sornette, and J.-R. Grasso (2003). Mainshocks are aftershocks of conditional foreshocks: how do foreshock statistical properties emerge from aftershock laws, *J. Geophys. Res.* **108,** no. B1, 2046.

Hough, S. E. and K. B. Olsen (Editors) (2007). Special issue on: regional earthquake likelihood models, *Seism. Res. Lett.* **78,** 7–140.

Kagan, Y. Y. (2004). Short-term properties of earthquake catalogs and models of earthquake source, *Bull. Seismol. Soc. Am.* **94,** no. 4, 1207–1228.

Kanamori, H., and D. L. Anderson (1975). Theoretical basis of some empirical relations in seismology, *Bull. Seismol. Soc. Am.* **65,** no. 5, 1073–1095.

Ogata, Y. (1988). Statistical models for earthquake occurrence and residual analysis for point processes, *J. Am. Stat. Assoc.* **83,** 9–27.

Ogata, Y. (1992). Detection of precursory relative quiescence before great earthquakes through a statistical model, *J. Geophys. Res.* **97,** 19,845–19,871.

Ogata, Y. (1998). Space-time point-process models for earthquake occurrences, *Ann. Inst. Statist. Math.* **50,** 379–402.

Ogata, Y., and H. C. Zhuang (2006). Space-time ETAS models and an improved extension, *Tectonophysics* **413,** 13–23.

Schoenberg, F. P. (2003). Multidimensional residual analysis of point process models for earthquake occurrences, *J. Am. Stat. Assoc.* **98,** 789–795.

Utsu, T., and A. Seki (1955). Relation between the area of aftershock region and the energy of the main shock, *J. Seismol. Soc. Jpn.* **7,** 233–240 (in Japanese).

Utsu, T., Y. Ogata, and R. S. Matsu'ura (1995). The centenary of the Omori formula for a decay of aftershock activity, *J. Phys. Earth* **43,** 1–33.

Wells, D. L., and K. J. Coppersmith (1994). New empirical relationships among magnitude, rupture length, rupture width, rupture area, and surface displacement, *Bull. Seismol. Soc. Am.* **84,** 974–1002.

Yamanaka, Y., and K. Shimazaki (1990). Scaling relationship between the number of aftershocks and the size of the main shock, *J. Phys. Earth* **38,** no. 4, 305–324.

Zhuang, J., Y. Ogata, and D. Vere-Jones (2004). Analyzing earthquake clustering features by using stochastic reconstruction, *J. Geophys. Res.* **109,** no. B5, B05301.

Zhuang, J. C., C. P. Chang, Y. Ogata, and Y. I. Chen (2005). A study on the background and clustering seismicity in the Taiwan region by using point process models, *J. Geophys. Res.* **110,** no. B5, B05S18.

GeoForschungsZentrum Potsdam
Section 2.1
Telegrafenberg, 14473 Potsdam, Germany
(S.H., B.E.)

Swiss Seismological Service
ETH Hoenggerberg
CH-8093 Zurich, Switzerland
(A.C.)

Manuscript received 18 October 2007